THE JOURNAL OF BIOLOGICAL CHEMISTRY
Vol. 278, No. 24, Issue of June 13, pp. 22031–22036, 2003
Printed in U.S.A.

A Complex II Defect Affects Mitochondrial Structure, Leading to *ced-3*- and *ced-4*-dependent Apoptosis and Aging*

Received for publication, November 7, 2002, and in revised form, March 31, 2003
Published, JBC Papers in Press, April 2, 2003, DOI 10.1074/jbc.M211377200

Nanami Senoo-Matsuda‡§, Philip S. Hartman¶, Akira Akatsuka‖, Shinichi Yoshimura‡, and Naoaki Ishii‡**

From the ‡Department of Molecular Life Science and the ‖Laboratory for Structure and Function Research, Tokai University School of Medicine, Isehara, Kanagawa 259-1193, Japan, §Tokyo Research Laboratories, Kyowa Hakko Kogyo Company Limited, Machida, Tokyo 194-8533, Japan, and the ¶Department of Biology, Texas Christian University, Fort Worth, Texas 76129

The *mev-1*(*kn1*) mutation of *Caenorhabditis elegans* is in Cyt-1, which encodes a subunit of succinate-coenzyme Q oxidoreductase in the mitochondrial electron transport chain. Mutants are hypersensitive to oxidative stress and age precociously in part because of increased superoxide anion production. Here, we show that *mev-1* mutants are defective in succinate-coenzyme Q oxidoreductase, possess ultrastructural mitochondrial abnormalities (especially in muscle cells), show a loss of membrane potential, have altered CED-9 and Cyt-1 protein levels under hyperoxia, and contain *ced-3*- and *ced-4*-dependent supernumerary apoptotic cells. These defects likely explain the failure of *mev-1* to complete embryonic development under hyperoxia as well as its reduced life span.

The oxidative phosphorylation system or electron transport chain is located within the mitochondrial inner membrane and is intimately responsible for three important processes: (i) ATP production, (ii) generation of reactive oxygen species (ROS),[1] and (iii) regulation of programmed cell death or apoptosis. The proximal ROS is superoxide anion ($O_2^{\cdot-}$), which derives from the Q cycle at rates estimated between 0.1 and 2% of the total electron flow (reviewed in Refs. 1 and 2). A variety of enzymatic and nonenzymatic defense mechanisms have evolved to either quench free radicals or ameliorate their resultant oxidative damage. Apoptosis (or programmed cell death) occurs by a mechanism that is conserved from nematodes to humans (reviewed in Refs. 3 and 4). In *Caenorhabditis elegans*, a largely invariant cell lineage (including 131 specific somatic cells destined to undergo apoptosis during hermaphroditic development) has provided fertile ground for the study of apoptosis. In other organisms, mitochondria are thought to provide a major initiation signal for apoptosis via the opening of the mitochondrial permeability transition pore, which leads to the release of a number of cell death-promoting factors, including cytochrome *c*. In *C. elegans*, normal, developmentally regulated apoptoses are not mediated by cytochrome *c* leakage from mitochondria. Mitochondrial oxidative phosphorylation system defects can cause a perplexing variety of diseases that exhibit a significant degree of clinical heterogeneity (reviewed in Refs. 5 and 6). For the most part, the pathophysiologies present themselves in tissues with high energy demands, such as heart and muscle. The interrelationship of the three activities described above (*e.g.* ATP generation, ROS production, and apoptosis initiation) may explain some of the perplexing pathophysiological features of mitochondrial diseases.

We have previously described the *mev-1*(*kn1*) mutant of the nematode *C. elegans* as containing a point mutation in Cyt-1 (a large subunit of cytochrome *b* in complex II) (7). Isolated by screening for hypersensitivity to oxidative damage (8), *mev-1* ages precociously at high oxygen concentrations and accumulates markers of aging (*e.g.* fluorescent materials and protein carbonyls) more rapidly compared with the wild type (9–11). We have recently shown that there are two distinct pathophysiologies in *mev-1* animals, *viz.* increased superoxide production from mitochondria and abnormal energy metabolism (12). Here, we report the results from histochemical and ultrastructural examinations of *mev-1* mutants that revealed severe defects in succinate-CoQ oxidoreductase and in the membrane potential ($\Delta\Psi_m$) of mitochondria. In addition, *mev-1* was found to possess morphological abnormalities in muscle mitochondria, particularly under hyperoxia. CED-9 and Cyt-1 protein levels were also abnormal in the *mev-1* mitochondrial membrane. This may explain our electron microscopic and Nomarski-DIC microscopic observations of supernumerary apoptosis in *mev-1* embryos. The abnormal apoptosis was suppressed by mutations in either *ced-3* or *ced-4*, indicating that the inappropriate signal in *mev-1* embryos stimulates induction of the normal *ced-9*/*ced-4*/*ced-3* apoptotic pathway. Furthermore, the *mev-1*,*ced-3* double mutant lived longer than *mev-1*, suggesting that the supernumerary apoptoses contribute to the phenotype of life shortening in *mev-1*.

EXPERIMENTAL PROCEDURES

General Methods and Strains—Culturing techniques have been described previously (13). PH126 (*ced-3*(*n1286*) *mev-1*(*kn1*) *unc-50*(*e306*)) was constructed by crossing MT3002 (*ced-3*(*n1286*)) hermaphrodites with *mev-1 unc-50* heterozygous males and scoring for second generation uncoordinated animals, who gave rise exclusively to third generation embryos with no apoptotic cells. PH137 (*ced-4*(*n1162*) *dpy-17*(*e164*) *mev-1*(*kn1*) *unc-50*(*e306*)) was constructed by crossing MT2551 (*ced-4*(*n1162*) *dpy-17*(*e164*)) hermaphrodites with *mev-1*(*kn1*) *unc-50*(*e306*) heterozygous males and picking Dpy Unc second generation progeny. Age synchronous populations were prepared as described previously (9–11). Hatching was determined as described previously (9–11). The life spans of individual adult hermaphrodites were determined on agar plates. To prevent progeny production, 5-fluoro-2′-deoxyuridine

* This work was supported in part by a grant-in-aid for aging research from the Ministry of Health, Labor, and Welfare of Japan and by grants from the Virtual Research Institute of Aging of Nippon Boehringer Ingelheim and the Mitsui Life Social Welfare Foundation. The costs of publication of this article were defrayed in part by the payment of page charges. This article must therefore be hereby marked "*advertisement*" in accordance with 18 U.S.C. Section 1734 solely to indicate this fact.

** To whom correspondence should be addressed. Tel.: 81-463-93-1121 (ext. 2575); Fax: 81-463-94-8884; E-mail: nishii@is.icc.u-tokai.ac.jp.

[1] The abbreviations used are: ROS, reactive oxygen species; CoQ, coenzyme Q; DIC, differential interference contrast.

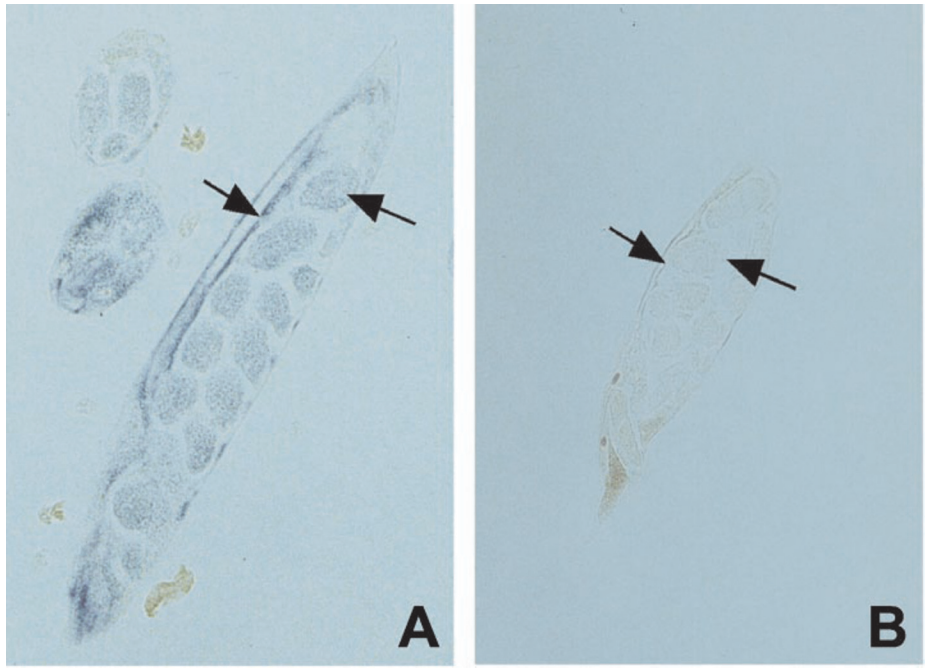

FIG. 1. **Succinate-CoQ oxidoreductase activity in wild-type and *mev-1 C. elegans*.** Immunocytochemistry was preformed to detect succinate-CoQ oxidoreductase activity *in situ*. Enzyme activity was readily apparent in the wild type (*A*), but virtually undetectable in the *mev-1* mutant (*B*). The *left* and *right arrows* point to body wall muscle and an embryo, respectively. Longitudinal sections are presented in both panels, with a cross-section also included in *A*.

(Sigma) was added to the nematode growth agar at a final concentration of 40 μM after animals had reached adulthood (14).

Histochemical Analysis of Succinate-CoQ Oxidoreductase—Young adults were embedded in Tissue-Tek O.C.T. compound (Miles Inc., Elkhart, IN) and stored at −80 °C until analyzed. Frozen cross-sections of 10 μm were cut on a cryostat at −20 °C; collected on glass slides; and incubated in 0.05 M sodium succinate, 0.05 M Tris-HCl (pH 7.4), and 0.5 mg/ml nitro blue tetrazolium chloride at 37 °C for 1 h to stain for succinate-CoQ oxidoreductase. The cross-sections were fixed in formaldehyde, dehydrated with a series of alcohols, and embedded in glycerol.

Electron Microscopy—Embryos and young adults were fixed overnight in 2.5% glutaraldehyde and 0.05 M phosphate buffer (pH 7.4) at room temperature. The samples were then washed with 0.1 M phosphate buffer (pH 7.4) and post-fixed in 1% OsO_4 and 0.05 M phosphate buffer (pH 7.4) for 1 h at 4 °C. After fixation, the samples were dehydrated with a series of alcohols and embedded in Quetol 812 (Nissin EM Ltd.). Thin sections were stained with 2% uranyl acetate and lead citrate and examined under a Joel 1200EX electron microscope operating at 80 kV.

Assay of $\Delta\Psi_m$—JC-1 (5,5′,6,6′-tetrachloro-1,1′,3,3′-tetraethylbenzimidazolylcarbocyanine iodide, catalog no. T-3168, Molecular Probes) was dissolved in Me_2SO at a concentration of 1 mg/ml. The JC-1 solution was added to newly hatched larvae in S basal buffer at 1 μg/ml and incubated in the dark for 10 min. After washing three times with S basal buffer, the animals were observed under a fluorescence microscope. Images were analyzed by Adobe Photoshop for emission characteristic of JC-1 monomers and aggregates.

Cell Corpse Assay—The mean numbers of cell corpses (mean ± S.D.) in comma stage embryos (~400 min after the first cleavage) (15) of wild-type, *mev-1*, and *mev-1,ced-3* animals were counted under Nomarski-DIC microscopy, examining for the signature raised appearance of apoptotic cells (18).

Preparation of Monoclonal Antibodies against Cyt-1 and CED-9—To raise antibodies, peptides were first synthesized using an automated peptide synthesizer. The peptides consisted of either amino acids 40–54 of *C. elegans* Cyt-1 or amino acids 206–223 of *C. elegans* CED-9 with an additional cysteine residue in the COOH terminus. The synthesized peptides were then conjugated to the adjuvant keyhole limpet hemocyanin (Calbiochem). Five-week-old female BALB/c mice were immunized four times by injection with 100 μg of keyhole limpet hemocyanin-conjugated Cyt-1 or CED-9 peptide. The serum antibody titers were determined by enzyme-linked immunosorbent assay. Spleens were removed 3 days after the final injection of the antigen, and 10^8 splenocytes were fused with 2×10^7 mouse myeloma P3U1 cells in the presence of polyethylene glycol 1000. Aliquots of the culture supernatants from the resultant hybridoma cells were screened by enzyme-linked immunosorbent assay and cloned twice by limited dilution to obtain monoclonal cell lines. Finally, stable clones showing anti-Cyt-1 (KM2408) or anti-CED-9 (KM2422) antibody activity were obtained. The hybridoma cells ($5–20 \times 10^6$) were injected intraperitoneally into 8-week-old female BALB/c nude mice, and monoclonal antibodies were purified from the ascites fluid.

Preparation of Mitochondrial Fractions for Western Blot Analysis—Young adults were harvested by centrifugation and washed five times with S basal buffer and once with isolation buffer (210 mM mannitol, 70 mM sucrose, 0.1 mM EDTA, and 5 mM Tris-HCl (pH 7.4)). The worms were homogenized (10%, w/v) in isolation buffer with a Teflon-glass homogenizer. Mitochondria were isolated by differential centrifugation at $600 \times g$ to remove debris and then at $7200 \times g$ to pellet mitochondria. Mitochondrial protein was measured using the BCA protein assay kit (Pierce).

Western Blot Analysis—Mitochondrial and cytosolic fractions were boiled in sample buffer (50 mM Tris-HCl (pH 6.8), 2% SDS, 0.14 M 2-mercaptoethanol, 10% glycerol, and 0.001% bromphenol blue) and separated by electrophoresis on 10 or 12.5% SDS-polyacrylamide gels. Proteins were electroblotted onto Immobilon polyvinylidene difluoride membranes in buffer consisting of 48 mM Tris, 39 mM glycine, 0.036% SDS, and 20% methanol and probed with 1 μg/ml KM2408 or 3 μg/ml KM2422. Immunoreactive proteins were visualized using the enhanced chemiluminescence system (ECL, Amersham Biosciences).

RESULTS

Succinate-CoQ Oxidoreductase Activity—Histochemical analysis of succinate-CoQ oxidoreductase activity was performed on frozen sections of wild-type and *mev-1* young adults (Fig. 1). Enzyme activity was widespread throughout wild-type animals, including embryos, with a concentration in body wall muscles. Conversely, there was a complete absence of staining in *mev-1* animals. This is consistent with the previous observation of reduced levels in *mev-1* cell extracts (7).

Ultrastructural Abnormalities in mev-1—Electron micrographs of wild-type body wall muscles revealed normal mitochondrial morphologies, including extensive cristae, at 21% oxygen (Fig. 2*A*) as well as at 50 and 10% oxygen (Fig. 2, *B* and *C*). Conversely, the mitochondria from *mev-1* body wall muscles had progressively disorganized cristae as oxygen was increased (Fig. 2, *D–F*). Many such mitochondria also contained electron-dense and amorphous inclusions at 21% oxygen (Fig. 2*D*), with additional paracrystalline inclusions apparent in animals reared under 50% oxygen (Fig. 2*E*). Similar ultrastructural abnormalities were present in hypodermal cells, including cuticles of *mev-1* (but not wild-type) animals (data not shown). These abnormalities did not appear at 10% oxygen (Fig. 2*F*).

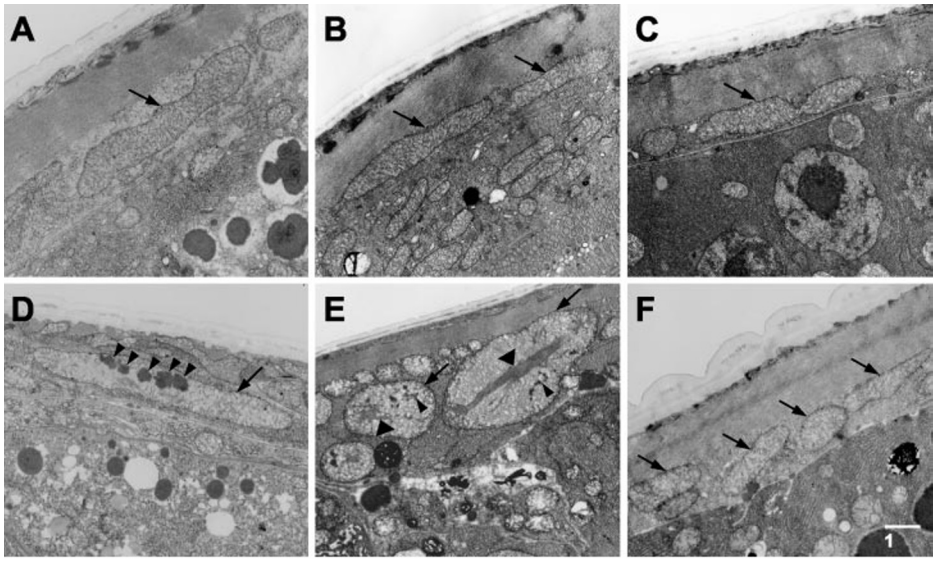

FIG. 2. **Electron micrographs of body wall muscle from wild-type and *mev-1* young adults.** Mitochondria in wild-type animals had normal morphologies, whereas those in *mev-1* animals had inclusion bodies under normoxia (21% oxygen) and hyperoxia (50% oxygen), but not under hypoxia (10% oxygen). *A–C* are micrographs from wild-type animals that had been grown under normoxia (21% oxygen), hyperoxia (50% oxygen), and hypoxia (10% oxygen), respectively. *D–F* are micrographs from *mev-1* mutants grown at 21, 50, or 10% oxygen, respectively. The *arrows* indicate some mitochondria. For the *mev-1* preparations, the *small arrowheads* indicate electron-dense and amorphous inclusions, whereas the *large arrowheads* indicate paracrystalline inclusions.

Similar ultrastructural changes also characterized *mev-1* intestinal cells. Although reasonably normal at 21% oxygen (Fig. 3*C*), *mev-1* intestinal mitochondria were noticeably swollen and rounded after animals were incubated under 50% oxygen (Fig. 3*D*). Unlike with *mev-1* mitochondria in muscle, no inclusion bodies were present. Again, hyperoxia had no detectable effect on the wild type (Fig. 2*B*). Is it possible that the more pronounced ultrastructural abnormalities in *mev-1* muscle *versus* intestinal tissue reflect the higher levels of oxidative phosphorylation in the former.

$\Delta\Psi_m$—The ability of mitochondria to generate a membrane potential was monitored by fluorescence microscopy after adding the dye JC-1. This dye is taken up by mitochondria as a monomer and forms J-aggregates when concentrated in highly polarized mitochondrial membranes. This transition is reflected by green fluorescence for monomers and by red fluorescence for dimers. In Fig. 4 (*A* and *B*), images of the wild type and *mev-1* loaded with JC-1 are shown, respectively. The image of *mev-1* showed a similar profile of monomers, but there were markedly fewer J-aggregates, indicating that $\Delta\Psi_m$ was significantly reduced in the *mev-1* mutant.

CED-9 and Cyt-1 Protein Levels Are Abnormal in mev-1 Mitochondria—Using antibodies raised against peptides that correspond to portions encoded by the *ced-9* and *cyt-1* genes, Western blotting was performed using mitochondrial preparations from wild-type and *mev-1* animals grown at different oxygen concentrations (Fig. 5*A*). Densitometric analyses revealed that the CED-9 and Cyt-1 protein levels were different in the two strains (Fig. 5*B*). The level of Cyt-1 in *mev-1* mitochondria was remarkably reduced under hyperoxia. In contrast, hyperoxia induced CED-9 protein levels in wild-type mitochondria, but caused a statistically insignificant reduction in *mev-1* mitochondria. The levels of *ced-9* and *cyt-1* mRNAs in the wild type and *mev-1* remained unchanged when oxygen was varied between 21 and 50% (data not shown); thus, the reduction of CED-9 and Cyt-1 protein levels in *mev-1* mitochondrial membranes may result from a structural abnormality of mitochondria.

Apoptosis, Embryogenesis, and Life Span—Given the importance of CED-9 in triggering apoptosis, its abnormal expression in *mev-1* suggested that this mutant might have an altered pattern of apoptosis. Indeed, the following data indicate that the *mev-1* mutation causes supernumerary embryonic apoptosis, especially under hyperoxia. Wild-type and *mev-1* embryos were scored using Nomarski-DIC microscopy at the "comma" stage (~400 min after the first cell division) for the presence of cells with the distinctive and easily recognizable raised and rounded morphology that characterizes apoptotic cells. The

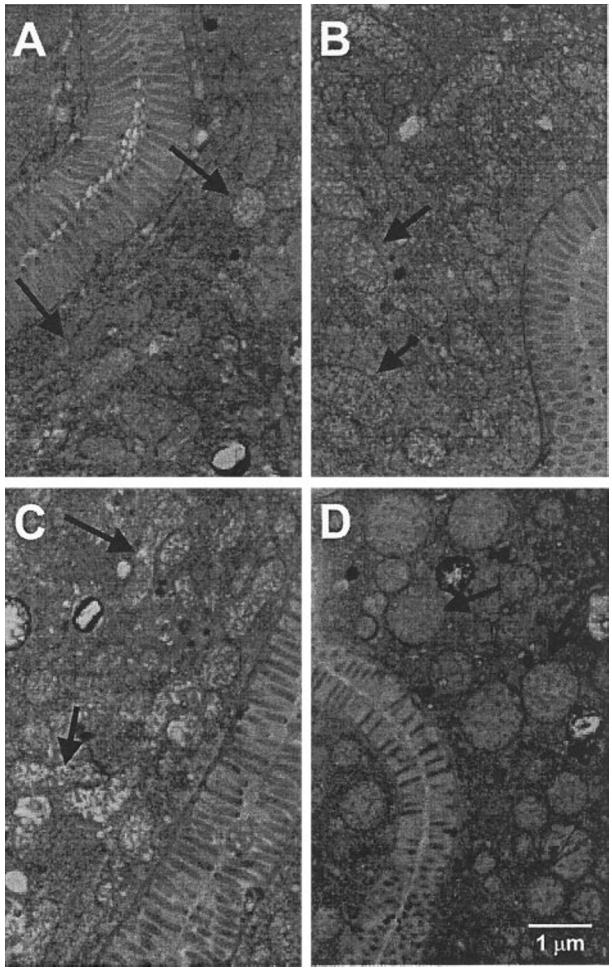

FIG. 3. **Electron micrographs of intestinal cells from wild-type and *mev-1* young adults.** As with mitochondria from body wall muscle (Fig. 2), there were significant differences between wild-type and *mev-1* intestinal mitochondria. *A* and *B* are micrographs of wild-type animals grown at either 21 or 50% oxygen, respectively. *C* and *D* are micrographs of *mev-1* mutants grown at 21 and 50% oxygen, respectively. The *arrows* indicate some mitochondria.

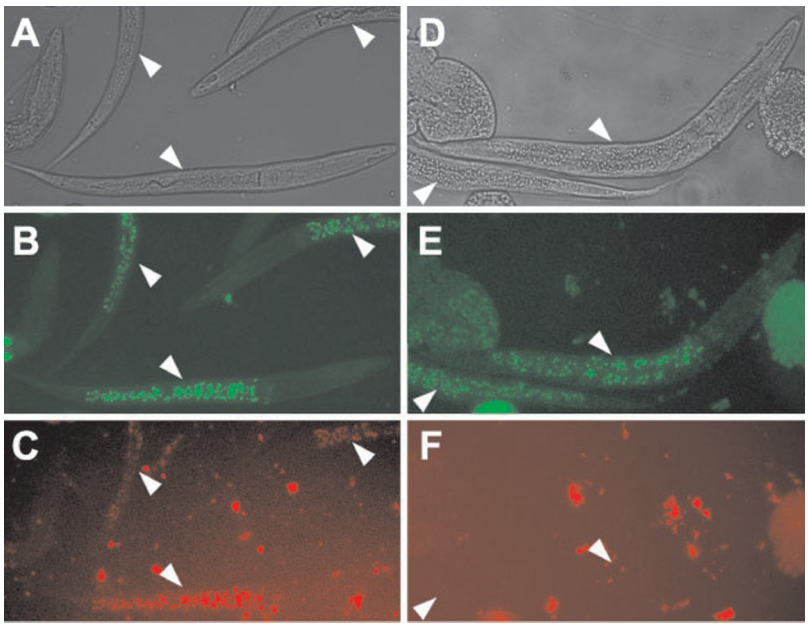

FIG. 4. **$\Delta\Psi_m$ as evidenced by JC-1-specific fluorescence in the wild type (*A–C*) and *mev-1* (*D–F*).** Three different images of the same preparation are shown for both the wild type (*A–C*) and *mev-1* (*D–F*). *A* and *D* are Nomarski-DIC images. *B* and *E* show green fluorescence at 530 nm (indicative of monomers). *C* and *F* show fluorescence at 690 nm (indicative of dimers). The *arrowheads* point to animals that were alive when this experiment was conducted. The differences in fluorescence intensity indicate substantial dysfunction in the mitochondrial membranes of *mev-1* animals. Most notably, there was significantly less red fluorescence in *mev-1* mitochondria, which indicates less membrane potential (*F*) than in the wild type (*C*). The eggs at the right ends of the *mev-1* panels were inviable, and therefore, that fluorescence was artifactual.

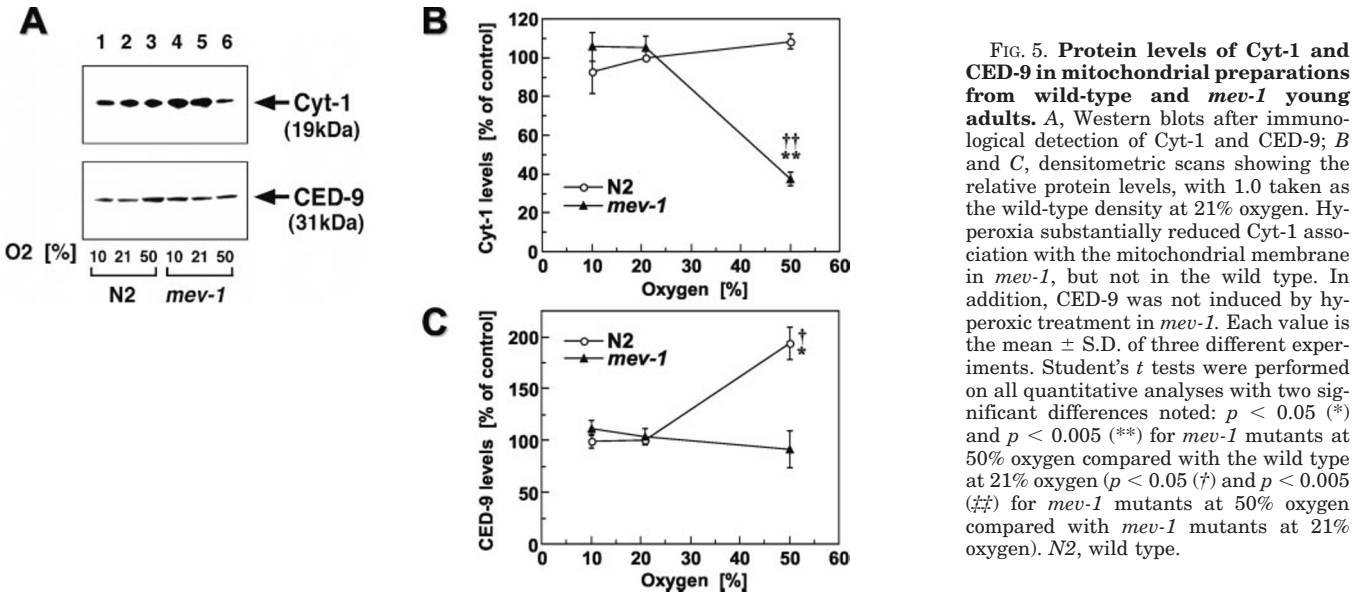

FIG. 5. **Protein levels of Cyt-1 and CED-9 in mitochondrial preparations from wild-type and *mev-1* young adults.** *A*, Western blots after immunological detection of Cyt-1 and CED-9; *B* and *C*, densitometric scans showing the relative protein levels, with 1.0 taken as the wild-type density at 21% oxygen. Hyperoxia substantially reduced Cyt-1 association with the mitochondrial membrane in *mev-1*, but not in the wild type. In addition, CED-9 was not induced by hyperoxic treatment in *mev-1*. Each value is the mean ± S.D. of three different experiments. Student's *t* tests were performed on all quantitative analyses with two significant differences noted: $p < 0.05$ (*) and $p < 0.005$ (**) for *mev-1* mutants at 50% oxygen compared with the wild type at 21% oxygen ($p < 0.05$ (†) and $p < 0.005$ (‡‡) for *mev-1* mutants at 50% oxygen compared with *mev-1* mutants at 21% oxygen). *N2*, wild type.

number of such cell corpses in *mev-1* embryos was >2-fold higher than in wild-type embryos (Fig. 6). The supposition that these were indeed supernumerary apoptoses is supported by the observation that null mutations in either *ced-3* or *ced-4* completely suppressed this (Fig. 6). These two genes are integral elements of the *ced-9*/*ced-4*/*ced-3* apoptotic pathway in *C. elegans* and are known to completely suppress the normal, developmentally regulated apoptoses for which this nematode is so well known. In addition to supernumerary apoptosis, we observed grossly malformed *mev-1* embryos that contained evidence of necrosis, particularly under hyperoxia (data not shown). As described previously (8), the life span of the *mev-1* mutant was shorter than that of the wild type (Fig. 7). The survival curve of the *mev-1*,*ced-3* double mutant was similar to that of the wild type during the first one-forth or so of life and then resembled that of *mev-1* during the later half (Fig. 7). This is numerically evidenced by the fact that the times needed to reduce survival to 80% were essentially identical in *mev-1*,*ced-3* (17.0 days) and the wild type (17.5 days), which were significantly longer than the 11.7 days for *mev-1*. Conversely, the times necessary to reduce survival to 20% were similar in *mev-1* (21.5 days) and *mev-1*,*ced-3* (21.4 days), but not in the wild type (25 days). Thus, a portion of the *mev-1*-specific reduction in life span was abrogated by a mutation that suppresses apoptosis, suggesting that the supernumerary apoptoses in *mev-1* contribute to its shortened life span.

As expected, the majority of wild-type animals completed embryonic development within 12 h after fertilization and hatched to become L1 larvae (Fig. 8). Conversely, hyperoxia negatively impacted this process in *mev-1* embryos (Fig. 8).

DISCUSSION

One of the greatest challenges in the molecular genetics era has been to elucidate the mechanisms by which specific mutations manifest themselves as phenotypic changes. This challenge increases significantly as one moves to progressively higher orders of biological organization. We have previously established that *mev-1*(*kn1*) is a missense mutation in a complex II subunit of the electron transport chain (7). Since that discovery, a significant challenge has been to account for the varied pathologies imposed by this mutation. We present them in the deliberate order below, reflecting the notion that each

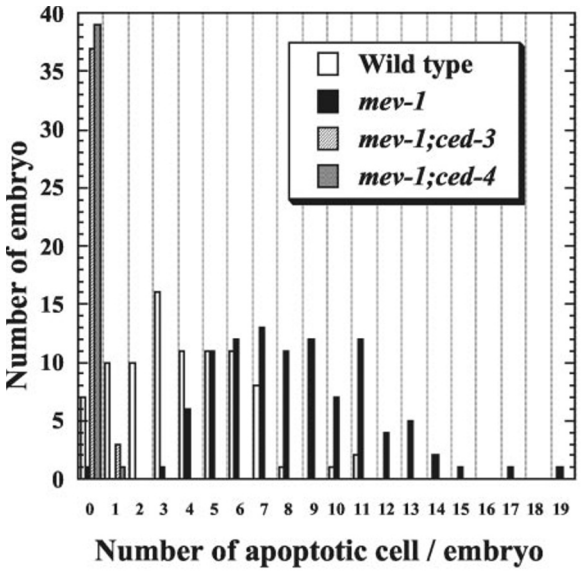

FIG. 6. **Number of apoptotic cells per embryo in comma stage embryos from wild-type, *mev-1*, *mev-1,ced-3*, and *mev-1,ced-4* young adults when grown at 21% oxygen.** Supernumerary apoptoses were present in *mev-1* embryos. Their suppression by loss-of-function mutations in *ced-3* and *ced-4* indicates that these are affected by the core apoptotic machinery of *C. elegans*.

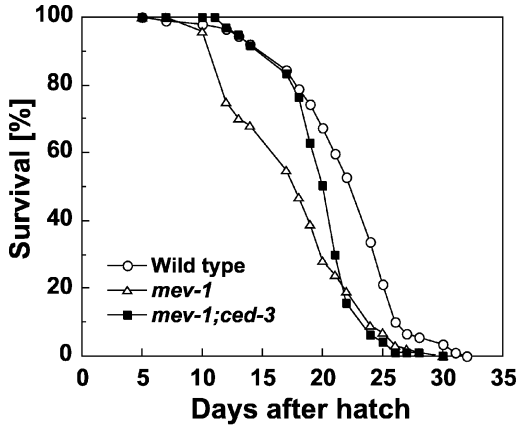

FIG. 7. **Life spans of the wild type, *mev-1*, and *mev-1,ced-3*.** Inclusion of the *ced-3* mutation, which suppresses apoptosis, caused a partial restoration of life span in *mev-1*. This suggests that the supernumerary apoptosis in *mev-1* contributes to its shortened life span.

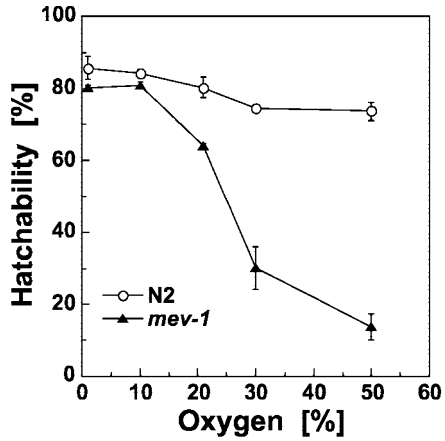

FIG. 8. **Effects of oxygen on embryonic development.** Percent hatchability denotes the percentage of embryos that successfully completed embryogenesis to hatch as L1 larvae. *N2*, wild type.

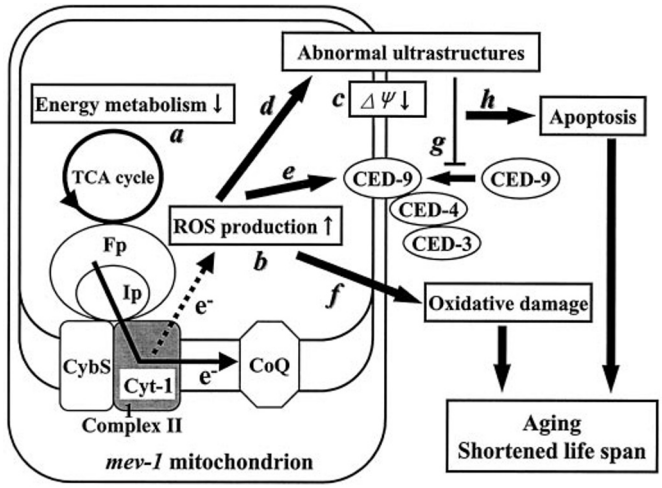

FIG. 9. **Model summarizing the manifestations of the *mev-1* mutation.** A defect in Cyt-1 results in the reduction of energy metabolism (*a*), ROS overproduction (*b*), and $\Delta\Psi_m$ (*c*). The ROS attack the mitochondrial membrane (*d*) and CED-9 protein (*e*) as well as any cellular components (*f*). The damaged and abnormal mitochondrial membrane prevents CED-9 binding to the mitochondrial membrane (*g*). The loss of function of mitochondria results in apoptosis (*h*). *TCA*, tricarboxylic acid; *Fp*, flavoprotein subunit; *Ip*, iron-sulfur; *CybS*; cytochrome *b*; e^-, electrons.

successive pathology is the consequence of those preceding it. First, it is clear that the *mev-1* mutation initially manifests itself as three distinct biochemical pathologies (12): (i) elevated ROS levels in *mev-1* mutants (specifically, superoxide anion levels in both intact mitochondrial and submitochondrial particles were approximately two times greater in *mev-1* mutants than in the wild type); (ii) depletion of the ROS scavenger glutathione in *mev-1* animals, which presumably renders *mev-1* animals more susceptible to the increased ROS levels mentioned above; and (iii) a higher ratio of lactate to pyruvate in *mev-1* mutants, suggesting that a metabolic imbalance known as lactate acidosis occurs in these animals. Second, these three biochemical pathologies, especially the first two, result in significantly higher levels of oxidative stress in *mev-1* animals, particularly in and around mitochondria. Third, this oxidative stress leads to perturbations in mitochondrial function that manifest as ultrastructural abnormalities, particularly under hyperoxic conditions (Figs. 2 and 3). These were more pronounced in body wall muscle than in intestinal cells, which presumably correlates with the relative rates of respiration and hence the levels of oxidative stress. Many electron-dense and amorphous inclusions at 21% oxygen (Fig. 2*D*) or additional paracrystalline inclusions apparent in animals reared under 50% oxygen (Fig. 2*E*) may be mitochondrial creatine kinase (16). Perhaps even more importantly, $\Delta\Psi_m$ was severely compromised in *mev-1* (Fig. 4). This suggests that the ultrastructural abnormalities lead to a loss of mitochondrial functionality in *mev-1* animals. It is also possible that the decreased $\Delta\Psi_m$ was not due to increased oxidative stress *per se*, but to another abnormal consequence of electron transport by the complex II defect in *mev-1*. Fourth, we have demonstrated that mitochondrially localized CED-9 protein levels are altered in a *mev-1* genetic background (Fig. 5). CED-9, the structural and functional homolog of Bcl-2, is a mitochondrially bound protein that controls apoptosis by regulating CED-4 and CED-3 activity (reviewed in Refs. 3 and 4). CED-9 was induced in wild-type mitochondria by hyperoxia, but this induction was not observed in *mev-1* mitochondria. As the mRNA levels of CED-9 and Cyt-1 were unchanged, the differences between the wild type and *mev-1* reflect some sort of post-translational

alteration. Again, it is possible that these differences are a secondary consequence of the increased oxidative stress that characterizes *mev-1.* Alternatively, they may reflect a more direct consequence of the *mev-1* mutation that acts to directly alter the mitochondrial membrane such that CED-9 cannot be properly retained. The lower amount of mitochondrially localized CED-9 in *mev-1* may in turn be insufficient to protect against the oxidative damage induced by hyperoxia. It is also possible that this MEV-1 protein may be destabilized in the mutant. Indeed, mRNA levels were unchanged, but this protein appeared only in mitochondria, not in the cytosol (data not shown). The increase in the CED-9 levels in the wild type may be due to up-regulation responding to oxidative stress, and *mev-1* may not have this ability. Fifth, the observation of supernumerary apoptosis in *mev-1* embryos (Fig. 6) is a logical and perhaps inevitable consequence of the pathologies articulated above. Its suppression by null mutations in either *ced-3* or *ced-4* indicates that, although the trigger is different from that normally employed by *C. elegans* during developmental pruning, the basic apoptotic machinery is the same. All of these pathologies ultimately explain two important organismal consequences of the *mev-1* mutation. The first was that *mev-1* embryos failed to complete development under hyperoxia. Increased oxidative stress, abnormal mitochondrial structure/function, and *ced-9*-mediated supernumerary apoptosis may all have contributed to this. The second of these organismal consequences was the shortened life span perpetrated by the *mev-1* mutation. Again, increased oxidation stress and abnormal mitochondrial structure/function may be important in this organismal phenotype. In addition, the ability of *ced-3* to partially restore the life span of *mev-1* to that of the wild type provides strong evidence that at least a portion of the reduced life span of *mev-1* animals is due to abnormal apoptosis. In summary, it is now possible to sort the various phenotypes associated with the *mev-1* mutation into a hierarchical scheme that progresses through increasing levels of biological complexity.

Finally, it is worth noting that three overlapping but distinct types of apoptosis have now been described in *C. elegans.* The first and most extensively explored is the developmentally regulated process in which specific cells are predestined to undergo programmed cell death in *C. elegans*. Specifically, 131 specific somatic cells are destined for apoptosis during normal development of hermaphrodites. Second, Gartner *et al.* (17) have described widespread apoptosis that can occur in the *C. elegans* germ line in response to DNA damage. Third, we have presented evidence of supernumerary apoptosis in somatic cells of *mev-1* embryos (Figs. 5 and 6), a likely consequence of the increased oxidative stress experienced by this mutant. There are a number of obvious similarities between these three types of apoptosis. First, they are morphologically similar (*i.e.* the apoptotic cells appear identical under Nomarski-DIC microscopy). Second, all three types of apoptosis are executed using the same core machinery, *i.e.* they are each dependent upon the *ced-9*/*ced-4*/*ced-3* gene products. There are also some clear differences between the three types of apoptosis. The first type of apoptosis is developmentally regulated and is restricted to specific cells in the lineage. It is not triggered by oxidative stress, having evolved as a "hardwired" characteristic to selectively eliminate specific cells in the *C. elegans* lineage. Conversely, the latter two are flexible and are responses to cellular damage. Both are likely evolutionary devices more akin to that in mammals, in which apoptosis serves as a mechanism to eliminate incapacitated cells that might threaten the whole organism (reviewed in Ref. 18). It is likely that both the *mev-1*-stimulated apoptosis and the germ line apoptosis share the same or similar triggering mechanisms as employed by mammals to eliminate grossly damaged cells. However, in addition to the fact that one involves somatic cells and the other a germ line, they exhibit genetic differences. Specifically, the germ line apoptosis requires functional *rad-5* and *him-7* gene products, *i.e.* DNA damage-induced germ line apoptoses do not occur in *rad-5* and *him-7* mutants (17). The *rad-5* and *him-7* mutants are not hypersensitive to oxidative stress, as is *mev-1*.[2] In addition, neither mutant shows supernumerary apoptoses in embryos.[2] Thus, it appears that the initial events that trigger these two types of apoptosis are different from one another. Further research will undoubtedly reveal more similarities and differences between these three types of apoptosis. As summarized in Fig. 9, the data in this and a previous report (12) go a long way toward clarifying the progressive consequences of the *mev-1* mutation.

Acknowledgments—We are indebted to Drs. K. Shibata and A. Furuya (Kyowa Hakko Kogyo Co. Ltd.) for preparing antibodies against the CED-9 and Cyt-1 proteins.

REFERENCES

1. Beckman, K. B., and Ames, B. N. (1999) *Physiol. Rev.* **78,** 547–581
2. Finkel, T., and Holbrook, N. J. (2000) *Nature* **408,** 239–247
3. Liu, Q. A., and Hengartner, M. C. (1999) *Ann. N. Y. Acad. Sci.* **887,** 92–104
4. Meier, P., Finch, A., and Evan, C. (2000) *Nature* **407,** 796–801
5. Morgan, J. A., and Hann M. G. (1999) *Biochim. Biophys. Acta* **1410,** 125–145
6. Wallace, D. G. (1999) *Science* **283,** 1482–1488
7. Ishii, N., Michikhiko, F., Hartman, P. S., Tsuda, M., Yasuda, K., Senoo-Matsuda, N., Yanases, S., Ayusawa, D., and Suzuki, K. (1998) *Nature* **394,** 694–697
8. Ishii, N., Takahashi, K., Tornita, S., Keino, T., Honda, S., Yoshino, K., and Suzuki, K. (1990) *Mutat. Res.* **237,** 165–171
9. Honda, S., Ishii, N., Suzuki, K., and Matsuo, M. (1993) *J. Gerontol.* **48,** B57–B61
10. Adachi, H., Fujiwara, Y., and Ishii, N. (1998) *J. Gerontol.* **53A**, B240–B244
11. Hosokawa, H., Ishii, N., Ishida, H., Ichimori, K., Nakazawa, H., and Suzuki, K. (1994) *Mech. Ageing Dev.* **74,** 161–170
12. Senoo-Matsuda, N., Yasuda, K., Tsuda, M., Ohkubo T., Yoshimura, S., Nakazawa, H., Hartman, P. S., and Ishii, N. (2001) *J. Biol. Chem.* **276,** 41553–41558
13. Brenner, S. (1974) *Genetics* **77,** 71–94
14. Mitchell, D. H, Stiles, J. W., Satelli J., and Sanadi, D. R. (1979) *J. Gerontol.* **35,** 28–36
15. Sulston, J. E., Schierenberg, E., White, J. G., and Thomson, N. (1983) *Dev. Biol.* **100,** 64–119
16. Stadhouders, A. M., Jap, P. H. K., Winkler, H.-P., Eppenberger, H. M., and Wallimann, T. (1994) *Proc. Natl. Acad. Sci. U. S. A.* **91,** 5089–5093
17. Gartner, A., Milstein, S., Ahmed, S., Hodgkin, J., and Hengartner, M. O. (2000) *Mol. Cell* **5,** 435–443
18. Evan, G., and Littlewood, T. (1998) *Science* **281,** 1317–1322

[2] P. S. Hartman, unpublished data.